Modeling the Rupture Dynamics of Strong Ground Motion (>1g) in Fault Stepovers

Holland Ladage (CSU Northridge), Julian Lozos (CSU Northridge), and Sinan Akçiz (CSU Fullerton)

Introduction and Motivation

Following the July 2019 Ridgecrest earthquakes, multiple field investigators noted that pebble- to boulder-sized rocks had been displaced from their place in the desert pavement in a compressional stepover along the right-lateral strike-slip M7.1 rupture trace. This suggests that localized ground accelerations exceeded 1 g, in contrast to instrumentally recorded ground accelerations which peak at ~0.7 g. Similar observations of displaced rocks concentrated in stepovers exist for the predominantly right-lateral strike-slip 2010 M7.2 El Mayor-Cucapah earthquake. Together, the Ridgecrest and El Mayor-Cucapah examples suggest that some aspect of how earthquake rupture negotiates a strike-slip fault stepover produces extremely localized strong ground acceleration.

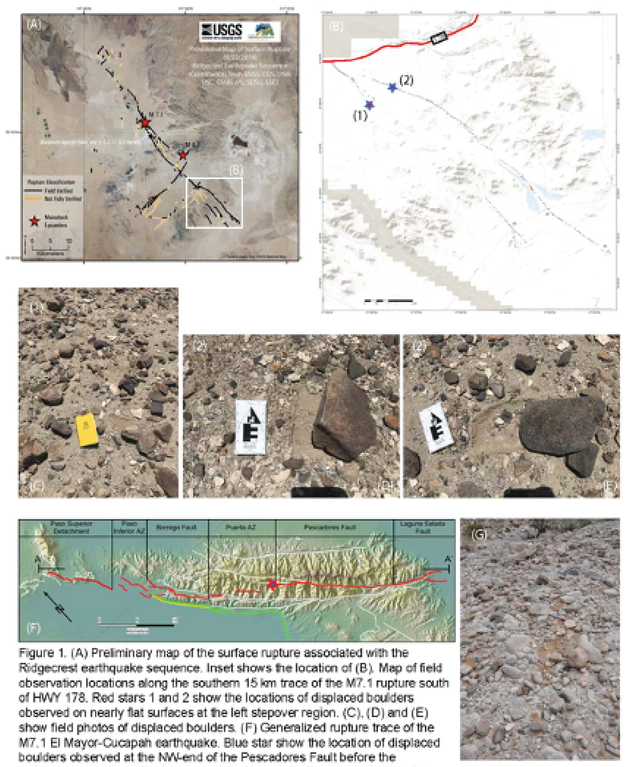

Figure 1. (A) Preliminary map of the surface rupture associated with the Ridgecrest earthquake sequence. Inset shows the location of (B). Map of field observation locations along the southern 15 km trace of the M7.1 rupture south of HWY 178. Red stars 1 and 2 show the locations of displaced boulders observed on nearly flat surfaces at the left stepover region. (C), (D) and (E) show field photos of displaced boulders. (F) Generalized rupture trace of the M7.1 El Mayor-Cucapah earthquake. Blue star show the location of displaced boulders observed at the NW-end of the Pescadores Fault before the distributed shearing within the many left stepover faults observed within the Puerta Accommodation Zone (map from Fletcher et al., 2010). (G) Field photo of the displaced boulders seen at the NW end of the Pescadores Fault.

Here, we conduct dynamic rupture simulations to investigate how the geometry of stepovers in strike-slip faults influences strong ground acceleration. In particular, we focus on how the amount of overlap between the two fault strands, and the width of the stepover, influences the location and intensity of the strongest ground motion, for both sub-shear and supershear rupture velocities. We only discuss compressional stepovers here, but we will be addressing extensional stepovers in the future.

Computational Method

We use the 3D finite element software FaultMod (Barall, 2009) to conduct our dynamic rupture simulations. We implement linear slip-weakening friction in a homogeneous fully-elastic half space. We nucleate our ruptures by raising the shear stress to over the yield stress at a chosen hypocenter (in this case, 3 km up and over from the lower left corner of the leftmost fault), then forcing propagation over an area larger than the critical patch size required for self-sustaining rupture.

We generate our fault meshes using the commercial software Cubit/Trelis. We discretize the mesh such that we model ground motion at 5 Hz in along the faults and within the stepover region.

We chose stress and material parameters consistent with previous work on stepovers (e.g. Harris and Day, 1993; Lozos et al., 2013).

Along-strike shear stress	40.0 MPa (subshear); 12.0 MPa (supershear)
Down-dip shear stress	0 MPa
Normal stress	66.6 MPa (subshear); 19.98 MPa (supershear)
Static coefficient of friction	0.75
Dynamic coefficient of friction	0.51 (subshear); 0.3 (supershear)
Slip weakening parameter	0.4 m
Vp	6000 m/s
Vs	3464 m/s
Density	2700 kg/m3
Hexahedral element size	55.55 m in near field, 500 m in far field
Radius of forced nucleation zone	3000 m

holland.ladage.368@my.csun.edu

julian.lozos@csun.edu

sakciz@fullerton.edu

Geometrical Parameter Space

Fault stepovers are complex regions, often with nonplanar geometry on the main strands, and many smaller faults within the stepover. Here, we isolate the effects of the primary stepover geometry: the strike-parallel overlap or separation between the two main fault strands, and the strike-perpendictular separation.

We model rupture on two planar right-lateral strike-slip faults, one 30 km long and one 10 km long, both with a seismogenic thickness of 12 km. We vary stepover width (strike-perpendicular separation) between 1 km and 5 km. For each stepover width, we also vary the strike-parallel position of the second fault from overlapping the first fault by 5 km to being 5 km separated from the first fault, at increments of 1 km.

Rupture Behaviors

We set our initial conditions such that the first (leftmost) fault always fully ruptures. From there, our simulations produced four different possible behaviors on the second (rightmost) fault.

Complete Rupture
The entire second fault slips.

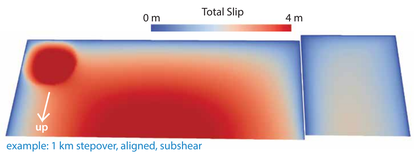

example: 1 km stepover, aligned, subshear

Partial Rupture
Only occurs in overlapping stepovers. The overlapping part of the second fault does not slip.

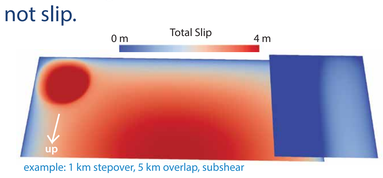

example: 1 km stepover, 5 km overlap, subshear

Triggered Slip
A small patch of triggered slip occurs at the top of the second fault, but a propagating rupture front does not develop.

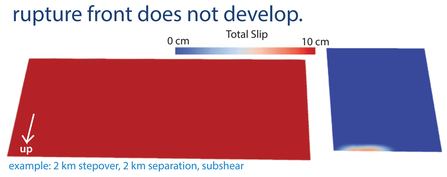

example: 2 km stepover, 2 km separation, subshear

No Slip
No portion of the second fault slips at all.

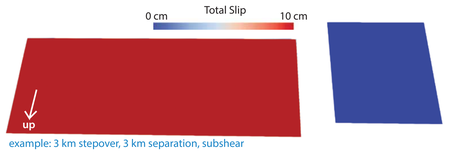

example: 3 km stepover, 3 km separation, subshear

These rupture patterns do change ground motion patterns in that ruptures which do involve the second fault also produce a ground motion signature along the second fault. However, this has little effect on peak ground motions, as discussed in the interpretation section below.

Ground Motion Results

Each combination of a stepover width and an overlap/separation distance represents one dynamic rupture simulation; a single simulation has five cells on the chart.

We color code magnitude (M) according to the rupture behaviors described above, and peak horizontal and vertical particle velocity (V_{Hmax} and V_{Vmax}) and particle acceleration (A_{Hmax} and A_{Vmax}) according to the color bars on the right. White spaces represent simulations we have yet to run. We will explore the same parameter space for extensional stepovers later on.

Supershear Ruptures Across Compressional Stepovers

	1 km stepover					2 km stepover					3 km stepover					4 km stepover					5 km stepover				
	M	V_{Hmax} m/s	V_{Vmax} m/s	A_{Hmax} g	A_{Vmax} g	M	V_{Hmax} m/s	V_{Vmax} m/s	A_{Hmax} g	A_{Vmax} g	M	V_{Hmax} m/s	V_{Vmax} m/s	A_{Hmax} g	A_{Vmax} g	M	V_{Hmax} m/s	V_{Vmax} m/s	A_{Hmax} g	A_{Vmax} g	M	V_{Hmax} m/s	V_{Vmax} m/s	A_{Hmax} g	A_{Vmax} g
5 km overlap	7	0.69	0.13	0.13	0.05																				
4 km overlap	7	0.69	0.13	0.13	0.05																				
3 km overlap	7.01	0.69	0.13	0.13	0.05																				
2 km overlap	7.01	0.69	0.13	0.13	0.05																				
1 km overlap	7.01	0.69	0.13	0.13	0.05																				
aligned	7.01	0.74	0.12	0.10	0.02	7.00	0.73	0.12	0.11	0.03	6.99	0.74	0.12	0.10	0.02	6.99	0.75	0.12	0.11	0.03	6.95	0.74	0.12	0.10	0.02
1 km separation	7.01	0.74	0.12	0.10	0.02	7.00	0.75	0.12	0.11	0.03	6.99	0.74	0.12	0.10	0.02	6.99	0.75	0.12	0.11	0.03	6.96	0.74	0.12	0.10	0.02
2 km separation	7.00	0.74	0.12	0.10	0.02	7.00	0.75	0.12	0.10	0.03	7.00	0.74	0.12	0.10	0.02	6.99	0.75	0.12	0.11	0.03	6.96	0.74	0.12	0.10	0.02
3 km separation	7.00	0.74	0.12	0.10	0.02	7.00	0.75	0.12	0.11	0.03	7.00	0.74	0.12	0.10	0.02	6.99	0.75	0.12	0.11	0.03	6.96	0.74	0.12	0.10	0.02
4 km separation	7.00	0.74	0.12	0.10	0.02	7.00	0.75	0.12	0.10	0.03	7.00	0.74	0.12	0.10	0.02	6.99	0.75	0.12	0.11	0.03	6.96	0.74	0.12	0.10	0.02
5 km separation	7.00	0.74	0.12	0.10	0.02	7.00	0.75	0.12	0.11	0.03	7.00	0.74	0.12	0.10	0.02	6.99	0.75	0.12	0.11	0.03	6.96	0.74	0.12	0.10	0.02

Subshear Ruptures Across Compressional Stepovers

	1 km stepover					2 km stepover					3 km stepover					4 km stepover					5 km stepover				
	M	V_{Hmax} m/s	V_{Vmax} m/s	A_{Hmax} g	A_{Vmax} g	M	V_{Hmax} m/s	V_{Vmax} m/s	A_{Hmax} g	A_{Vmax} g	M	V_{Hmax} m/s	V_{Vmax} m/s	A_{Hmax} g	A_{Vmax} g	M	V_{Hmax} m/s	V_{Vmax} m/s	A_{Hmax} g	A_{Vmax} g	M	V_{Hmax} m/s	V_{Vmax} m/s	A_{Hmax} g	A_{Vmax} g
5 km overlap	6.99	0.78	0.22	0.18	0.05																				
4 km overlap	7.01	0.78	0.22	0.18	0.08																				
3 km overlap	7.02	0.78	0.22	0.18	0.05																				
2 km overlap	7.02	0.78	0.22	0.18	0.08																				
1 km overlap	7.02	0.78	0.22	0.18	0.05	6.97	0.82	0.22	0.27	0.13	6.98	0.78	0.22	0.18	0.05	6.98	0.84	0.22	0.27	0.14	6.97	0.78	0.22	0.20	0.05
aligned	7.03	0.77	0.22	0.18	0.05	6.98	0.79	0.22	0.19	0.05	6.98	0.78	0.22	0.14	0.03	6.98	0.79	0.22	0.20	0.05	6.98	0.78	0.22	0.15	0.03
1 km separation	7.03	0.78	0.22	0.14	0.03	6.98	0.80	0.22	0.22	0.07	6.98	0.78	0.22	0.14	0.03	6.98	0.80	0.22	0.17	0.06	6.98	0.79	0.22	0.15	0.04
2 km separation	7.02	0.77	0.22	0.15	0.04	6.98	0.79	0.22	0.19	0.05	6.98	0.78	0.22	0.14	0.03	6.98	0.79	0.22	0.20	0.05	6.98	0.78	0.22	0.14	0.04
3 km separation	7.02	0.78	0.22	0.14	0.03	6.98	0.80	0.22	0.22	0.07	6.98	0.78	0.22	0.14	0.03	6.98	0.80	0.22	0.17	0.06	6.98	0.79	0.22	0.15	0.04
4 km separation	6.98	0.77	0.22	0.14	0.03	6.98	0.79	0.22	0.19	0.05	6.98	0.78	0.22	0.14	0.03	6.98	0.79	0.22	0.20	0.05	6.98	0.78	0.22	0.14	0.04
5 km separation	6.98	0.78	0.22	0.14	0.03	6.98	0.80	0.22	0.21	0.07	6.98	0.78	0.22	0.14	0.03	6.98	0.80	0.22	0.17	0.06	6.98	0.79	0.22	0.15	0.04

2nd Fault Behavior
- Complete Rupture
- Partial Rupture
- Triggered Slip
- No Slip

Max. Particle Velocity (m/s)
- 0.00 - 0.20
- 0.21-0.40
- 0.41-0.60
- 0.61-0.80
- 0.81+

Max. Particle Acceleration (g)
- 0.00-0.05
- 0.06-0.10
- 0.11-0.15
- 0.16-0.20
- 0.21+

For supershear ruptures, the stepover geometry (and whether or not rupture jumps the stepover) seems to make no significant difference in peak ground velocities or accelerations.

For subshear ruptures, there is a slightly more noticeable variation in values across geometrical parameter space, but the difference is still a matter of less than 10 cm/s and less than 0.05 g.

Both supershear and subshear ruptures produce comparable particle velocities, but subshear ruptures cause slightly stronger accelerations overall. That said, none of the ground accelerations in our simulation come even close to the 1 g we infer is necessary to displace boulders.

Interpretation (So Far)

For supershear ruptures, the stepover geometry has a negligible effect on peak ground motion because the largest velocities and (particularly) accelerations occur at the point of the supershear transition along the first fault. The mach cone pattern associated with supershear rupture also results in motion at the end of the first fault directing diagonally away from, rather than toward, the stepover.

For subshear ruptures, the largest velocities and accelerations do occur in the stepover region. They are generated by the stopping phase from rupture hitting the end of the first fault (e.g. Harris and Day, 1993). The slight fluctuation in peak values is likely related to how much stress from the stopping phase immediately does (or does not) activate the second fault (e.g. Lozos et al., 2015).

Maximum Ground Motion Distributions, 1 km stepover, 3 km separation

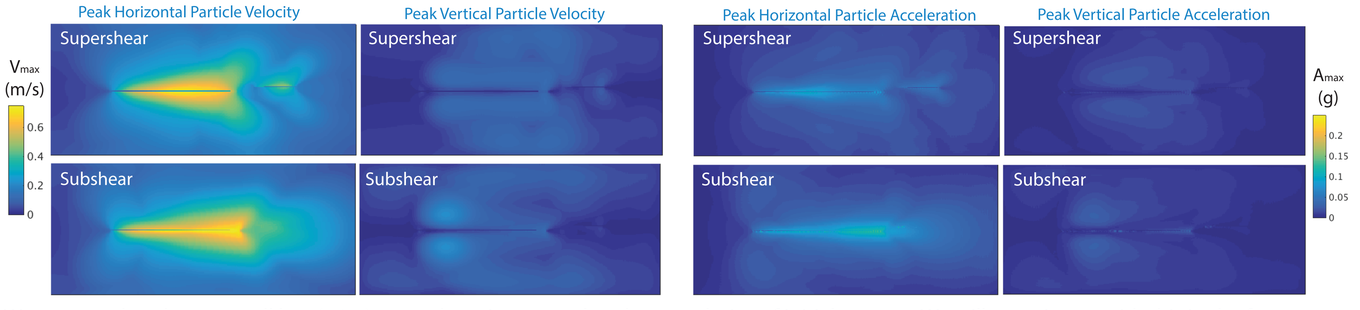

We suspect that these overall low (<1 g) ground motions are related to our choice of initial stresses. We will experiment with this in the future.

What's Next?

- Finish running these compressional stepover simulations.
- Explore the same parameter space for extensional stepovers.
- Investigate which stress/material/rupture velocity conditions are necessary to produce >1 g ground accelerations in the stepover region.
- Also consider other possible mechanisms for the displaced boulders.

References

- Barall, M. (2009). A grid-doubling finite-element technique for calculating dynamic three-dimensional spontaneous rupture on an earthquake fault. Geophysical Journal International, 178(2), 845-859.
- Harris, R. A., & Day, S. M. (1993). Dynamics of fault interaction: Parallel strike-slip faults. Journal of Geophysical Research: Solid Earth, 98(B3), 4461-4472.
- Lozos, J. C., Oglesby, D. D., & Brune, J. N. (2013). The effects of fault stepovers on ground motion. Bulletin of the Seismological Society of America, 103(3), 1922-1934.
- Lozos, J. C., Oglesby, D. D., Brune, J. N., & Olsen, K. B. (2015). Rupture Propagation and Ground Motion of Strike-Slip Stepovers with Intermediate Fault Segments. Bulletin of the Seismological Society of America, 105(1), 387-399.

This project is funded by SCEC Award #20199.